Polarization-dependent properties of the cladding modes of a single mode fiber covered with gold nanoparticles

Wenjun Zhou,[1,*] David J. Mandia,[2] Matthew B.E. Griffiths,[2] Aliaksandr Bialiayeu,[1] Yang Zhang,[1] Peter G. Gordon,[2] Seán T. Barry,[2] and Jacques Albert[1]

[1]*Department of Electronics, Carleton University, Ottawa, Ontario K1S 5B6, Canada*
[2]*Department of Chemistry, Carleton University, Ottawa, Ontario K1S 5B6, Canada*
[*]*wenjun_zhou@carleton.ca*

Abstract: The properties of the high order cladding modes of standard optical fibers are measured in real-time during the deposition of gold nanoparticle layers by chemical vapor deposition (CVD). Using a tilted fiber Bragg grating (TFBG), the resonance wavelength and peak-to-peak amplitude of a radially polarized cladding mode resonance located 51 nm away from the core mode reflection resonance shift by 0.17 nm and 13.54 dB respectively during the formation of a ~200 nm thick layer. For the spectrally adjacent azimuthally polarized resonance, the corresponding shifts are 0.45 nm and 16.34 dB. In both cases, the amplitudes of the resonance go through a pronounced minimum of about 5 dB for thickness between 80 and 100 nm and at the same time the wavelengths shift discontinuously. These effects are discussed in terms of the evolving metallic boundary conditions perceived by the cladding modes as the nanoparticles grow. Scanning Electron Micrographs and observations of cladding mode light scattering by nanoparticle layers of various thicknesses reveal a strong correlation between the TFBG polarized transmission spectra, the grain size and fill factor of the nanoparticles, and the scattering efficiency. This allows the preparation of gold nanoparticle layers that strongly discriminate between radially and azimuthally polarized cladding mode evanescent fields, with important consequences in the plasmonic properties of these layers.

OCIS codes: (060.2310) Fiber optics; (060.3735) Fiber Bragg gratings; (160.4236) Nanomaterials; (240.0310) Thin films.

References and links

1. J. J. Mock, R. T. Hill, Y.-J. Tsai, A. Chilkoti, and D. R. Smith, "Probing dynamically tunable localized surface plasmon resonances of film-coupled nanoparticles by evanescent wave excitation," Nano Lett. **12**(4), 1757–1764 (2012).
2. L. Tong, V. D. Miljković, and M. Käll, "Alignment, rotation, and spinning of single plasmonic nanoparticles and nanowires using polarization dependent optical forces," Nano Lett. **10**(1), 268–273 (2010).
3. Y.-C. Lu, R. Geng, C. Wang, F. Zhang, C. Liu, T. Ning, and S. Jian, "Polarization effects in tilted fiber Bragg grating refractometers," J. Lightwave Technol. **28**(11), 1677–1684 (2010).
4. J. Albert, L.-Y. Shao, and C. Caucheteur, "Tilted fiber Bragg grating sensors," Laser Photon. Rev. (early view), http://onlinelibrary.wiley.com/doi/10.1002/lpor.201100039/abstract.
5. Y. Shevchenko, C. Chen, M. A. Dakka, and J. Albert, "Polarization-selective grating excitation of plasmons in cylindrical optical fibers," Opt. Lett. **35**(5), 637–639 (2010).
6. C. Caucheteur, Y. Shevchenko, L.-Y. Shao, M. Wuilpart, and J. Albert, "High resolution interrogation of tilted fiber grating SPR sensors from polarization properties measurement," Opt. Express **19**(2), 1656–1664 (2011).
7. J. Pollet, F. Delport, K. P. F. Janssen, K. Jans, G. Maes, H. Pfeiffer, M. Wevers, and J. Lammertyn, "Fiber optic SPR biosensing of DNA hybridization and DNA-protein interactions," Biosens. Bioelectron. **25**(4), 864–869 (2009).

8. T. Schuster, R. Herschel, N. Neumann, and C. G. Schaffer, "Miniaturized long-period fiber grating assisted surface plasmon resonance sensor," J. Lightwave Technol. **30**(8), 1003–1008 (2012).
9. A. Bialiayeu, C. Caucheteur, N. Ahamad, A. Ianoul, and J. Albert, "Self-optimized metal coatings for fiber plasmonics by electroless deposition," Opt. Express **19**(20), 18742–18753 (2011).
10. L.-Y. Shao, J. P. Coyle, S. T. Barry, and J. Albert, "Anomalous permittivity and plasmon resonances of copper nanoparticle conformal coating on optical fibres," Opt. Mater. Express **1**(2), 128–137 (2011).
11. T. J. J. Whitehorne, J. P. Coyle, A. Mahmood, W. H. Monillas, G. P. A. Yap, and S. T. Barry, "Group 11 amidinates and guanidinates: potential precursors for vapour deposition," Eur. J. Inorg. Chem. **2011**(21), 3240–3247 (2011).
12. C.-F. Chan, C. Chen, A. Jafari, A. Laronche, D. J. Thomson, and J. Albert, "Optical fiber refractometer using narrowband cladding-mode resonance shifts," Appl. Opt. **46**(7), 1142–1149 (2007).
13. I. Del Villar, I. R. Matias, F. J. Arregui, and M. Achaerandio, "Nanodeposition of materials with complex refractive index in long-period fiber gratings," J. Lightwave Technol. **23**(12), 4192–4199 (2005).
14. C. Caucheteur, C. Chen, V. Voisin, P. Berini, and J. Albert, "A thin metal sheath lifts the EH to HE degeneracy in the cladding mode refractometric sensitivity of optical fiber sensors," Appl. Phys. Lett. **99**(4), 041118 (2011).
15. The cylindrical Finite Difference Fiber Mode Solver included in FIMMWAVE by Photon Design, http://www.photond.com/products/fimmwave/fimmwave_features_25.htm
16. I. Horcas, R. Fernández, J. M. Gómez-Rodríguez, J. Colchero, J. Gómez-Herrero, and A. M. Baro, "WSXM: A software for scanning probe microscopy and a tool for nanotechnology," Rev. Sci. Instrum. **78**(1), 013705 (2007).
17. M. Chen and R. G. Horn, "Refractive index of sparse layers of adsorbed gold nanoparticles," J. Colloid Interface Sci. **315**(2), 814–817 (2007).
18. W.-J. Lee, J.-E. Kim, H. Y. Park, S. Park, M.-S. Kim, J. T. Kim, and J. J. Ju, "Optical constants of evaporated gold films measured by surface plasmon resonance at telecommunication wavelengths," J. Appl. Phys. **103**(7), 073713 (2008).
19. E. Castanié, V. Krachmalnicoff, A. Cazé, R. Pierrat, Y. De Wilde, and R. Carminati, "Distance dependence of the local density of states in the near field of a disordered plasmonic film," Opt. Lett. **37**(14), 3006–3008 (2012).
20. S. H. Choi, B. Kwak, B. Han, and Y. L. Kim, "Competition between excitation and emission enhancement of quantum dots on disordered plasmonic nanostructures," Opt. Express **20**(15), 16785–16793 (2012).
21. P. S. Westbrook, T. A. Strasser, and T. Erdogan, "In-line polarimeter using blazed fiber gratings," Photonics Technol. Lett. **12**(10), 1352–1354 (2000).
22. Q. Bao, H. Zhang, B. Wang, Z. Ni, C. H. Y. X. Lim, Y. Wang, D. Y. Tang, and K. P. Loh, "Broadband graphene polarizer," Nat. Photonics **5**(7), 411–415 (2011).

1. Introduction

The interaction between propagating light waves and nanometer-sized gold particles presents many interesting features that have been studied in several contexts [1,2]. It is therefore expected that depositing gold nanoparticles on the cladding of an optical fiber will have an impact on the cladding-guided modes of such fibers and may lead to new applications in sensing, all optical switching, and nonlinear optics. Tilted fiber Bragg gratings (TFBGs) are ideally suited for such studies because of their capability to excite a number of cladding modes whose properties can be probed very precisely by measuring the wideband spectral response of the grating transmission [3,4]. Furthermore, due to the breakup of the circular symmetry caused by the tilted grating planes, the polarization state of the incident core mode controls the orientation and polarization of the excited cladding modes at the cladding boundary [4]. This is of utmost importance for metal coatings as the boundary conditions for metal-dielectric interfaces depend very strongly on the polarization state of the light. For example, cladding modes with radial polarization at the cladding boundary can be excited selectively and be used to couple light into surface plasmon waves on metal coated fibers. A gold-coated TFBG refractometer based on Surface Plasmon Resonance (SPR) was demonstrated using this technique [5], and shown to yield a great enhancement in the minimum surrounding refractive index (SRI) detection level [6], compared to non-TFBG fiber SPR devices [7,8]. In all these fiber-based SPR configurations the quality and uniformity of the (typically) 50 nm thick metal layer is critical but also difficult to control; especially to make it uniform around the circumference of the fiber. The gold coatings in the papers mentioned above were fabricated by sputtering or evaporation techniques, which require fiber rotations to obtain approximately uniform films. Better uniformity gold films are expected from conformal coating approaches such as electroless plating and chemical vapor

deposition (CVD) which have been demonstrated for gold and copper respectively [9,10]. Recently, a new precursor for gold CVD was developed [11] and the present work deals with an investigation of the effect of this new CVD coating process on the properties of the cladding modes of such coated fibers. As shown in Fig. 1, we used single-ended 10° tilt TFBGs inserted in the CVD process chamber and monitored their transmission spectrum from the input side by using the reflection from a gold mirror deposited on the fiber end. This avoids having to loop back the fiber inside the chamber. The wavelengths and amplitudes of resonances associated with cladding modes of different polarization states were obtained throughout the CVD process. The observations obtained from inside the fiber using the TFBG resonances were compared with scanning electron microscope images of the films at various stages of deposition, and with infrared camera images of the light scattered out of the fiber by the nanoparticles. The results indicate three different regimes according to the density and thickness of the CVD gold nanoparticle coatings. In particular, during the coating process we observed a well-defined transition between isolated nanoparticles and a semi-continuous film that has a strong impact on the optical properties of the optical fiber cladding modes.
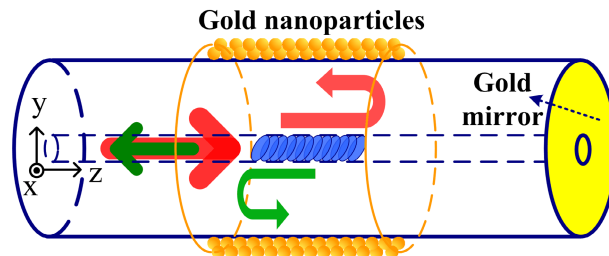

Fig. 1. Schematic diagram of TFBG coated by gold nanoparticles (the arrows show how the incident core guided light (red) goes through the grating twice, each time coupling light to cladding modes). The light remaining in the core (straight green arrow) returns to the interrogation system.

2. Principle and sensor fabrication

In order to clarify how nanoscale metal coatings influence cladding mode resonances, a brief review of TFBG properties is required before the description of the experiments. A periodical refractive index perturbation with tilted grating planes along the core axis couples the forward-propagating core mode to a number of backward-propagating cladding modes in addition to a backward-propagating core mode (the "Bragg" mode). The wavelength of the resonance of the Bragg mode, λ_{Bragg} and of the ith order cladding mode resonance $\lambda_{cladding}^{i}$ in the transmission spectrum of TFBG can be expressed as [12]

$$\lambda_{Bragg} = 2Neff_{Bragg}\Lambda / \cos\theta \qquad (1)$$

$$\lambda_{cladding}^{i} = (Neff_{Bragg}^{i} + Neff_{cladding}^{i})\Lambda / \cos\theta \qquad (2)$$

where $Neff_{Bragg}$ is the effective index of core mode at the Bragg wavelength, Λ is the grating period, θ is the tilt angle of the grating planes, $Neff_{Bragg}^{i}$ and $Neff_{cladding}^{i}$ are the effective indices of the core mode and ith cladding mode at the wavelength of the ith cladding resonance. The guiding properties of these cladding modes and hence of $Neff_{cladding}$ depend on the permittivity of the medium in which the cladding is located. Therefore we expect the wavelengths of the cladding mode resonances to shift during the deposition of gold nanoparticles on the fiber. The amplitudes of these cladding resonances would also change under the influence of the imaginary part of the complex refractive index of gold (as shown for LPGs in [13]) and of the loss due to scattering by the nonuniform layer of nanoparticles on the surface of the TFBG.

We further expect these effects to depend strongly on the polarization state of the cladding modes at the cladding boundary. The tilted grating planes break the azimuthal symmetry of the fiber and two orthogonal polarization states of the electrical field input light can be defined relative to the tilt plane: S-polarized light with the electrical field perpendicular to y-z plane and P-polarized light with the electrical field parallel to y-z plane (as shown in Fig. 1). In previous reports, we showed that when the polarization state of the light at the TFBG contains only S- or P-polarized light (two extreme cases), the electrical field of the excited high order cladding modes also has radically different polarization properties [5,14]. Simulations obtained with a finite difference mode solver [15], and shown in Fig. 2, indicate that S-polarized light can only couple into high order cladding modes that have their electrical field tangential to the cladding boundary, while P-polarized light excites cladding modes with predominantly radial electrical fields. This difference is highlighted in Fig. 3, where two transmission spectra of the same grating under S- and P-polarized light interrogation (measured in air without coating) show clearly different sets of resonances that occur in closely spaced pairs. Similarly to TFBGs with uniform thin metal layers, we use this polarization selectivity to obtain additional information about the gold nanoparticle coating as it grows.
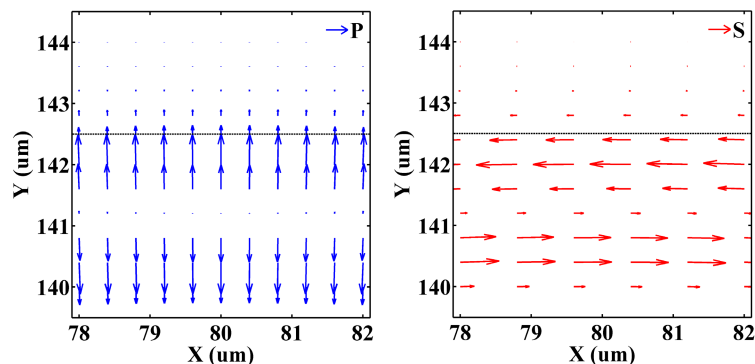

Fig. 2. Simulated electrical fields of a high-order cladding mode excited by P- (left) and S- (right) polarized light. The figures represent a small area of 4 by 4 μm^2 close to cladding boundary (indicated by a horizontal line at Y = 142.5 μm). All results were calculated with FIMMWAVE.

The TFBGs were written in hydrogen-loaded photosensitive CORNING SMF-28 fiber with a pulsed KrF excimer laser using the phase-mask method. The Bragg wavelength is around 1610 nm so that important cladding modes are observed in the middle of the C-band (near 1550 nm). The length of TFBG is only 4 mm long in order to minimize the impact of eventual coating thickness non-uniformities on the grating response. A tilt angle of 10° leads to a large number of strong, high order cladding mode resonances that have larger evanescent field penetration outside the cladding. In order to have a single entry port in the furnace used for the CVD process and to avoid bending the fiber, a reflective sensing configuration of TFBG was implemented by cleaving the fiber 1.5 cm downstream from the TFBG and coating the end with a sputtered gold mirror (Fig. 1). This configuration further enhances the response of the TFBG since core-guided light goes through the grating twice. The gold mirror at the downstream end was prepared separately by conventional sputtering, and its thickness (several microns) is such that the addition of more gold on the fiber end (during the nanoparticle deposition process) has no effect on its reflectance. There is unavoidable growth on the fiber end but it has no influence on the properties of the cladding modes at the location of the grating (a few cm away).
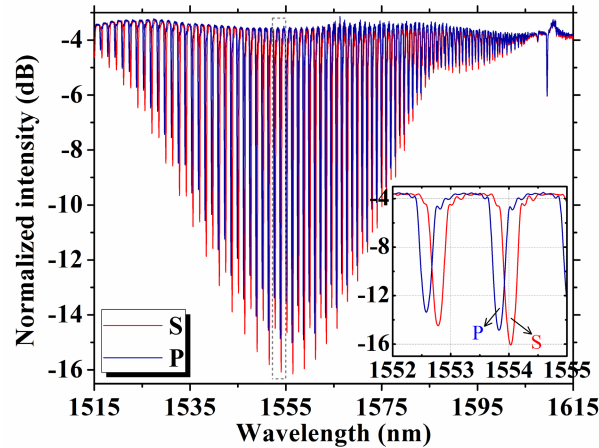
Fig. 3. Experimental transmission spectra of 10° TFBG with S- and P-polarized input light in air, inset: detailed spectra from 1550 to 1556 nm.

3. Experiment and results

Figure 4 illustrates the experimental setup of the gold CVD system and the in situ spectral measurement system. The fiber was fixed on a metal boat and the end containing the TFBG was inserted into a vial filled with a single-source gold precursor ($[Au(NiPr)_2CNMe_2]_2$) [11].
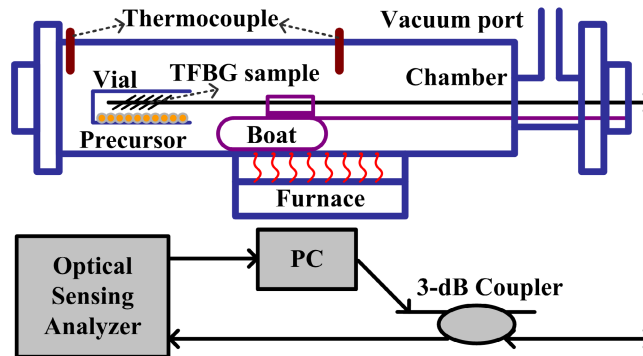

Fig. 4. Schematic diagram of gold CVD system and spectral monitoring setup. The optical sensing analyzer includes a scanning laser source with a wavelength range from 1520 to 1570 nm and a synchronized photodetector.

The fiber and vial were located in a deposition chamber made of stainless steel, the chamber itself being located within a heating furnace. At the beginning of the experiment the chamber was pumped down to a base pressure of 30 mTorr and then the furnace temperature ramp (11 °C/min) program was set to 255 °C. Since the reaction chamber is situated far from the main thermocouple, temperature measurements were collected on a second thermocouple fitted further down the furnace tube to account for any thermal lag. As the temperature increases, it reaches the vaporization and decomposition point of the highly volatile precursor (~220 °C) and the gold nanoparticles begin to nucleate on all exposed surfaces including the cladding of the TFBG. EDS analysis performed on the fibers and planar samples with this gold compound showed no significant or detectable impurities (only signals for Si, O, and Au). The process self-terminates when the precursor has fully reacted and the furnace is then allowed to cool down. The whole process takes about 10 minutes and the onset of the deposition itself occurs after approximately 8 minutes, as corroborated by changes in the TFBG response. With this methodology, the final thickness of the gold nanoparticle coating

on the fiber is determined by the amount of precursor in the vial. For instance, the film thickness from a 30 mg sample of precursor was typically ~200 nm. In other experiments wherein the mass was varied, a linear relationship was found with respect to the film thickness, and a nominal growth rate of 5 nm/s (starting from onset of deposition) was calculated from *ex situ* thickness calculations using WSXM 5.0 image processing software [16]. Finally, the impact of the strong temperature changes on the spectral positions of the resonances was removed from the data analysis by recording the wavelength shift of the Bragg mode and subtracting it from the shifts of the cladding modes. The Bragg mode is well isolated from the cladding boundary (therefore from any effect resulting from the deposition) and it has been verified that all cladding mode resonances have the same intrinsic temperature dependence as the Bragg mode [12]. It must be noted that this deposition configuration yields coatings that vary in thickness as a function of distance from the precursor source. We usually work with longer TFBGs (between 10 and 20 mm long) in order to have narrower resonances to enhance the Q-factor and thus the minimum detectable level of sensors, but if the coating thickness varies over this length, the net effect is a chirp of the grating properties and widening of resonances. Also, we need only to deposit the particles on the fiber sections where the grating is located, because these are the only locations where light is emitted into the cladding.
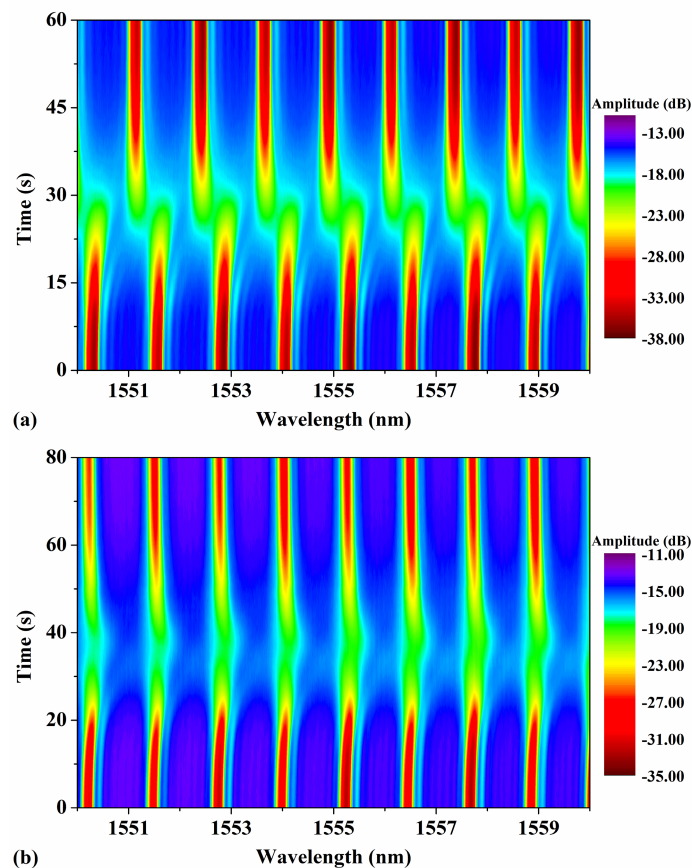

Fig. 5. TFBG spectral evolutions of during gold nanoparticles deposition under S- (a) and P-polarized (b) light (the color scale represent the amplitude of the resonances). Spectra are acquired every second and temperature-corrected with reference to the Bragg mode shifts.

Before the deposition, the polarization of the incident light was adjusted to the exact S- or P-polarization state using an electronic polarization controller (PC) (JDS Uniphase) that contains one polarizer, a half-wave plate and a quarter-wave plate. This combination allows the preparation of arbitrary polarization states at the fiber input, which can compensate for any change of polarization state induced by fiber loops and twists in the optical path leading to the TFBG. The optimum launch polarization is simply determined by observing the transmission spectrum and maximizing either one of the two sets of transmission resonances. The spectral evolution was recorded continually during the deposition by an optical sensing analyzer (Micron Optics Si720) with a measurement frequency of 5 Hz. Even though S and P polarized spectra were obtained during separate experiments, it was verified that the results were reproducible for identical process parameters.

Figure 5 shows the evolution of the TFBG reflective transmission ranging from 1550 to 1560 nm (where the cladding modes have the largest amplitudes for 10° TFBG) with S- and P-polarized light. The origin of the time scale in Fig. 5 is determined by the moment when the precursor begins to evaporate, as indicated by a small pressure rise in the chamber (near 8 minutes into the process, as mentioned above). Basically, both the S- and P-polarized spectra go through a similar evolution in that all cladding modes become much attenuated at first, and then re-grow back to a shape very similar to the original one measured in air. There are subtle differences however: the initial attenuation occurs faster and lasts longer for P-polarized light, but most importantly the re-appearance of the resonances as the thickness increases is accompanied by a strong wavelength shift for S-polarized light but hardly any at all for the P-polarized case. This is further clarified in quantitative terms by plotting the amplitude and wavelength of one pair of resonances near 1559 nm as shown in Fig. 6.
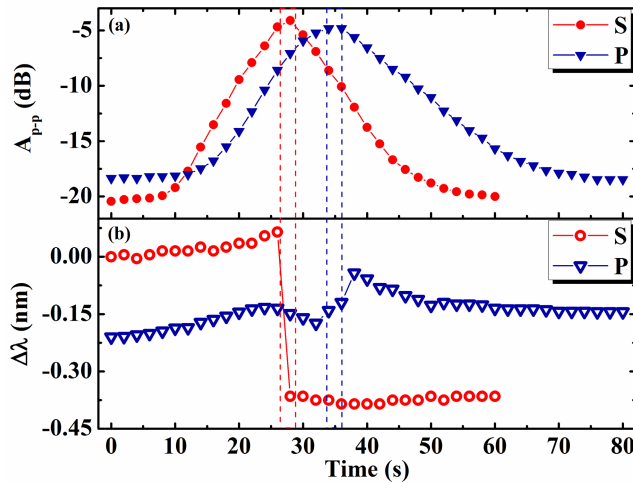

Fig. 6. Normalized amplitude (a) and wavelength (b) evolutions versus time of gold deposition under S- and P-polarized light. The vertical dashed lines bound the minimum amplitudes for each polarization, highlighting the simultaneous occurrence of the corresponding wavelength change discontinuities.

The results indicate that the amplitudes of S-resonances decrease by 15 dB in the first 25 s of deposition and recover completely after 60 s. Still in the first 25 seconds, the resonance wavelength red-shifts by about ~0.08 nm. Most importantly, near the minimum amplitude point the wavelength discontinuously blue-shifts by ~0.4 nm and stays relatively constant for the remainder of the deposition, as the resonance gradually regains its full amplitude. The P-resonances also decrease in amplitude but by a slightly smaller amount and about 10 seconds later than the minimum of the S-resonance. The most significant difference however is that the wavelength shift of P-resonances is completely antagonistic to that of the S-resonance: it

first increases slowly by about 0.06 nm, then decreases by 0.05 nm and when the amplitude minimum is reached near the 35 second point, jumps discontinuously upward by 0.14 nm. The net result is that there is an interchange of the S- and P-resonances during the deposition. This confirms our previous finding, obtained for continuous, 50 nm-thick sputtered gold films [6] that the S- and P- resonances were interchanged between air-clad and metal-clad fibers.

In order to further investigate the origin of the results obtained, we obtained scanning electron microscopy (SEM) images of the surface morphology of the gold nanoparticles deposited on three TFBG samples with different amounts of precursor in the vial (yielding different thicknesses and shorter process durations). Figure 7 shows the surface morphology of the growing gold film at beginning (a), middle (b), and end (c) of the whole TFBG spectral evolution, as determined by comparing the final TFBG spectra with those of the "full" process shown in Figs. 5 and 6. Also included (Fig. 7(d)) is an image of one of the fiber cross sections that were obtained to estimate the average coating thickness for each case. This correlation yields average thicknesses of 50, 100, and 200 nm for films equivalent to process durations of 20, 35, and 80 seconds on Fig. 7 (i.e. before the point of maximum attenuation, near the maximum and, finally later in the deposition). Average grain sizes were measured from SEM images to grow linearly with time from 55+/–3 nm at 21 seconds, to 122+/–10 nm at 50 seconds. Individual grains become difficult to identify beyond that time. The films are all quite rough but the metal coverage increases from very sparse (46.41%), to relatively dense (72.92%) (but with gaps remaining), and finally to complete, although with a rough top surface. Finally, two further TFBGs were prepared with thicknesses corresponding to deposition times of 20 s and 40 s, i.e. when the coated TFBG have the largest amplitude differences between S- and P-resonances according to Fig. 6.

The last two gratings were used to investigate how much of the cladding guided light was scattered by the coatings under these circumstances. We used a broad band source (BBS), polarization controller, and optical spectrum analyzer (OSA) to achieve spectra with precise S- and P-polarized input light, and then imaged the IR-scattering emitted at right angle from the fiber axis with an infrared camera. The measured spectra and associated IR-scattering
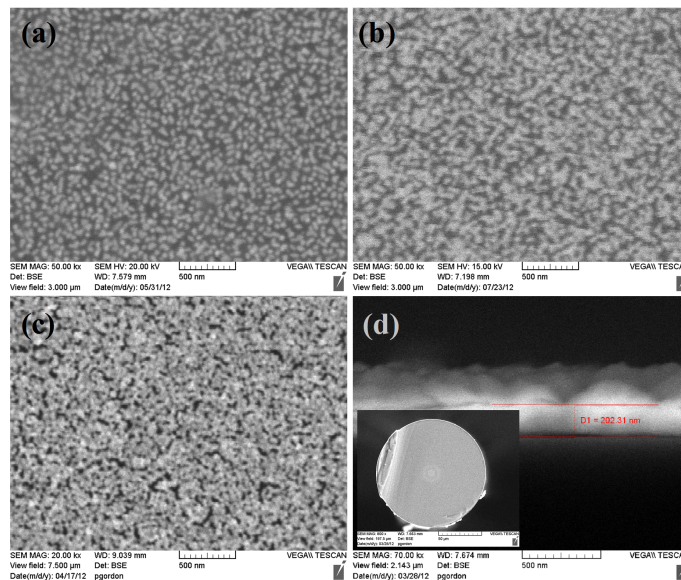

Fig. 7. SEM images of gold nanoparticles deposited on the TFBG surface with different deposition times (with a scale of 500 nm). (a) Beginning, (b) middle, and (c) end of TFBG spectral evolution. (d) Sectional image of gold film in a small area with an inset of coated TFBG sectional view.
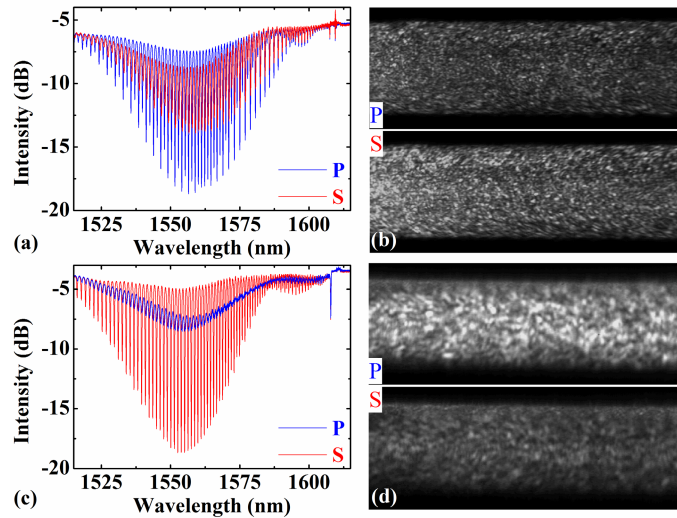
Fig. 8. Reflective transmission spectra and IR-scattering images under S- and P-polarized lights of the coated TFBG with spectral response times of ~20 s (a), (b) and 40 s (c), (d).

images with S- and P-polarized light are shown in Fig. 8. By comparing the spectra and the images of the two TFBGs, it is very clear that there is a strong correlation between the scattered light intensity and attenuation of the TFBG resonances (the brightest scattering occurring for Fig. 8(c), P-polarization, that also shows the strongest resonance amplitude attenuation). In comparison, uncoated TFBGs with similar grating periods look totally dark at these wavelengths because the evanescent field of cladding modes is non-radiative in the direction away from the fiber surface.

4. Discussion

It is now clear that the attenuation of the amplitudes is mostly due to scattering by the metal nanoparticles rather than absorption of light by the metal. Furthermore we can extrapolate this finding by claiming that the full recovery of the resonance amplitudes (both S- and P-polarized) arises when the coatings "fill up" and no longer allow the light to leak out (this spectral recovery was also observed for thick electro-plated gratings in [9]. The almost full recovery of the resonance amplitudes also confirm that very little energy is dissipated in the metal itself, otherwise the resonances would remain lossy, losing amplitude and increasing in spectral width as a result.

The peculiar wavelength shift differences observed between the two polarization states can be explained by the granular nature of the films grown. Based on previous reports about the anomalous permittivity of thin metallic film [10,17,18], the real part of the complex refractive index of a thin film composed of gold nanoparticles increases significantly above the value for bulk gold (a value near 0.55 at these wavelengths) when the particle densities are sparse and the sizes are small. So during the initial growth of the nanoparticles, a thin material layer with a relatively large average refractive index is formed on the cladding, resulting in a red-shift of both kinds of cladding mode resonances. Recalling from elementary electromagnetic theory that tangential fields cannot penetrate high-conductivity metals, S-polarized light (tangential to the cladding surface) can only exit the cladding through the gaps in the coating, while P-polarized light (normal to the interface) can tunnel across the gold particles and also exits from the air gaps. In order to confirm this idea and get a deeper insight into the experimentally observed process, the solution of the full problem of the interaction of the evanescent field of various cladding modes with the films shown in Fig. 7 will require exhaustive additional investigations. In the meantime, in order to validate some of the

hypotheses brought forth to explain our experimental results, 2D-finite difference time domain (FDTD) numerical simulations of a much simplified configuration were carried out (with software from Lumerical Solution, Inc.). We modeled a linear array of conducting disks with a diameter of 40 nm and a center-to-center spacing of 50 nm (Fig. 9). The disks were surrounded with air and had a complex refractive index $(n + ik)$ of $0.51 + i10.8$. The simulation domain was meshed with cells on a 0.2 nm grid. The incident electromagnetic field was a plane wave pulse centered at wavelength of 1.5 μm with its electric field vector **E** lying in the plane of the simulation domain. Two orthogonal cases were investigated: a) wave incident from the bottom of the image with the vector E oriented horizontally (corresponding to azimuthally polarized modes, from S-polarization coupling); b) wave incident from the left with the vector **E** oriented vertically (approximating a radially polarized evanescent field, i.e. a mode generated by P-polarized light).

The optical intensity distributions around the metal disks under these two excitation conditions are shown in Fig. 9. It is very clear that the light with the electric field tangential to the nanoparticle layer (S-polarization) is strongly localized between the metal particles but is forbidden to go through the particles themselves. On the other hand, light associated with P-polarized excitation of the TFBG (case b) has strong electric field maxima on the top and bottom of the nanoparticles while being "forbidden" in between because it is polarized tangentially to the metal there (and the gap is too narrow). Given these simulated results, we can infer that as the particles grow and the air gaps decrease, light from S-polarized resonances reaches a point, when most of the gaps between particles close, where it can no longer penetrate the nanoparticle coating and becomes bounded by what appears from the inside of the fiber as a continuous (i.e. bulk) metal film with a low refractive index of 0.5, hence the large sudden blue shift of the resonances. On the other hand, when the air gaps close the P-resonances continue to probe deeply into the metal and to continue to red shift slowly as long as their evanescent field can tunnel across the whole layer thickness (apart from some irregular behavior in the transition zone where the gaps become small before closing). The net result is that the presence of the nanoparticles introduces loss for the
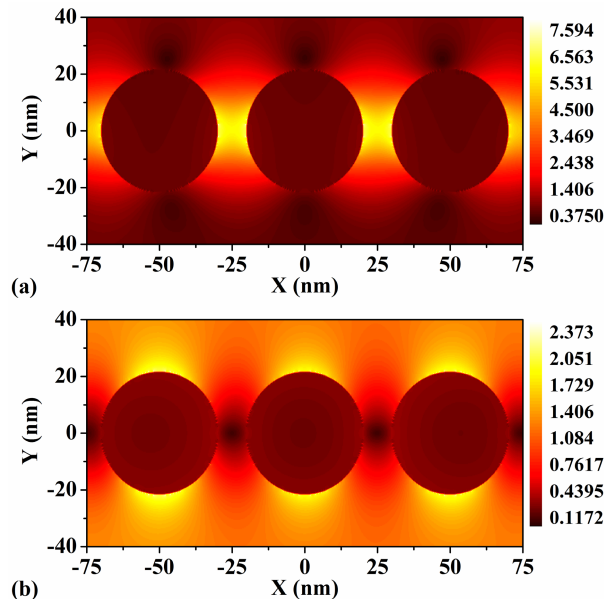

Fig. 9. Simulated intensity distributions of electric fields on single layer gold nanoparticles interacted by S- (a) and P-polarized (b) light in free space. The incident light propagates along Y-axis in S case, while along X-axis in P case.

cladding modes propagating underneath. This loss is reflected in the attenuation of the cladding mode resonances (they become less pronounced, as seen on Figs. 5, 6, and especially Fig. 8(c)). Figure 8 clearly shows that most of the attenuation arises because of scattering, by opposition to absorption by the metal. If absorption was involved, the resonances would not recover their full amplitudes (see Fig. 6(a)) as the films become continuous and thicker. Finally, for the most strongly attenuated cladding modes (and strongest scattered light), the total net loss of the core guided mode for P-polarized light (as determined by its transmission spectrum) is only about 5 dB: this means that about 70% of the light is extracted from the core and transferred to the nanoparticles and their surroundings.

Regardless of the validity of these hypotheses, the main conclusion remains that we have identified, from the TFBG spectral signature, the conditions where the HE (and TE) cladding modes become isolated from the fiber surroundings while allowing EH (and TM) modes to tunnel across and scatter efficiently off the nanoparticles.

5. Conclusion

We have demonstrated that there is a significant correlation between the near infrared polarized transmission spectra of 10° TFBG inscribed in standard single mode fibers and the optical properties gold particle coatings with thicknesses ranging from zero to ~200 nm, and formed using a recently developed chemical vapor deposition process. In particular we identified spectral signatures corresponding to coatings yielding different states of light confinement, scattering, and polarization. For instance, for films with particle sizes near 50 nm and 100 nm respectively we can selectively scatter out of the fiber light polarized predominantly azimuthally or radially and thus control the plasmonic enhancement properties due to these disordered nanostructured metal films [19,20]. However, the optimum film thickness and uniformity will vary from application to application and the scattering properties further depend on the size of individual nanoparticles and the porosity of the films, parameters that cannot be controlled independently at the present time with this method. What we show here is that the film thickness can be controlled by stopping the deposition before the precursor is exhausted and that several film conditions can be obtained as a result. Further experiments with different process temperatures, residual pressure in the chamber, or additional reactants would provide a richer parameter space but the results obtained so far are sufficient for developing interesting devices. It is to be pointed out that the purpose here was not to control the polarization of the guided light, as can be done very efficiently using un-coated TFBGs with large tilt angles [21], or by using graphene coatings on side polished fibers for instance [22], but rather to excite coatings on fibers with radially or azimuthally polarized light at infrared wavelengths. As a side benefit, we have also confirmed the usefulness of the TFBG as a process monitor for thin film coatings of CVD gold on other substrates in the same process chamber, in situ and in real time.